


## Increases in the temperature seasonal cycle indicate long-term drying trends in Amazonia

Paul D. L. Ritchie<sup>1</sup>  , Isobel Parry<sup>1</sup>, Joseph J. Clarke<sup>1</sup>, Chris Huntingford<sup>2</sup>  & Peter M. Cox<sup>1</sup> 

Earth System Models project a wide range of rainfall changes in the Amazon rainforest, and hence changes in soil moisture and evapotranspiration. Hydrological changes are heterogeneous, meaning local measurements are too sparse to constrain projections of large-scale hydrological change. Here we show that changes in the amplitude of the temperature seasonal cycle are strongly correlated with annual mean evaporative fraction (surface latent heat flux as a fraction of surface net radiation) changes, across reanalyses and Earth System Model projections. We find an increase in annual temperature amplitude of 1 °C is associated with a reduction in evaporative fraction of up to 0.04. The observed temperature seasonal cycle amplitude increase (0.4 °C) over the last three decades implies Amazon drying, determined in the absence of soil or energy flux measurements, matches Earth System Model simulations of the recent past. Additionally, Earth System Models predict further temperature seasonal cycle amplitude increases, suggesting drying will continue with future climate change.

<sup>1</sup>College of Engineering, Mathematics and Physical Sciences, University of Exeter, Exeter, UK. <sup>2</sup>UK Centre for Ecology and Hydrology, Wallingford, UK.  
email: [Paul.Ritchie@exeter.ac.uk](mailto:Paul.Ritchie@exeter.ac.uk)

The Amazon rainforest has historically been one of the largest carbon pools on Earth, storing up to 200 petagrams of carbon (PgC)<sup>1</sup>. Furthermore, the Amazon rainforest has acted as a strong carbon sink, whereby from 1990–2007 the rainforest had an annual carbon uptake of 0.42–0.65 PgC yr<sup>-1</sup><sup>2,3</sup>, helping to offset CO<sub>2</sub> emissions caused by the human burning of fossil fuels. However, due to climate change and deforestation, the Amazon rainforest could already have changed from a carbon sink to a carbon source<sup>4</sup>. Further warming, and more importantly, drying, could potentially trigger the system into tipping to an alternative state<sup>5,6</sup>. Although the possibility of Amazon dieback has been strongly debated and previously considered to be model dependent<sup>7</sup>, there is evidence to suggest a greater agreement amongst the latest CMIP6 generation of climate models. In particular, 5 of 7 CMIP6 models with dynamic vegetation display localised abrupt areas of dieback over the Amazon region caused by warming and drying associated with elevated CO<sub>2</sub> levels alone (and not changes in land use)<sup>8</sup>.

The length of the dry season over southern Amazonia has increased in recent decades<sup>9,10</sup>, and has been accompanied by a prolonged fire season<sup>11</sup>. Specifically, the frequency of dry days has increased with a reduction in rainfall during September–November<sup>12</sup>. Hot extremes show an increasing trend as does the number of consecutive dry days<sup>13</sup>. The observed drying has been found to be outside the range of trends due to natural variability and is instead caused by elevated greenhouse gas levels and deforestation<sup>14</sup>. Importantly, tropical tree growth links strongly to dry season rainfall<sup>15</sup>. Therefore, as a result of these drier and longer dry seasons, over three-quarters of the rainforest has been reported as losing resilience since the early 2000's, consistent with an approaching critical threshold<sup>16</sup>.

Drying of Amazonia will be revealed by changes in evaporation. Evaporation can be measured with eddy covariance<sup>17</sup>, but there is a paucity of such sites across South America, and those available are often limited in their period of operation<sup>18</sup>. However, changes to evaporation level also alter near-surface meteorology. More than half of the precipitation that falls in the Amazon basin is created by its own evaporation and transpiration<sup>19</sup>. Due to these high levels of evaporation, tropical rainforests tend to be cooler than more open land despite their lower albedo<sup>20</sup>. For that reason, we hypothesise that changes to the amplitude of the temperature seasonal cycle, defined as the difference in minimum and maximum monthly means for the year, will reveal changes to water availability especially in the dry season.

The previous generation of CMIP5 climate models have shown increases in temperature variability that are associated with

decreases in evaporative fraction (the fraction of the surface net radiation which is returned to the atmosphere as the latent heat flux due to evapotranspiration), especially in the southern hemisphere<sup>21</sup>. Other studies<sup>22,23</sup> have also linked temperature variability with the evaporative fraction. A strong negative correlation has previously been established in CMIP5 models, between the ratio of the change in the annual hottest day relative to the change in the local average temperature, and the evaporative fraction for the Amazon<sup>24</sup>. However, the CMIP5 models show a large range in temperature variability over the Amazon, typically with a substantial positive model bias compared to reanalyses<sup>21</sup>. An improvement to the temperature seasonal cycle amplitude bias<sup>25</sup>, as well as improved representation of evapotranspiration over the Amazon region in the latest CMIP6 generation of climate models<sup>26</sup>, provides motivation to establish similar relationships in this study. A further extension in this study is to apply the derived relationships with observational temperature data, for which records are of greater temporal and spatial resolution, to estimate the amount of Amazon drying since 1900. We base our analysis on projections by a large ensemble of CMIP6 climate models and data from the ERA5 reanalysis product<sup>27</sup>, which acts as our source of observationally-derived data.

## Results

We first consider time series data from the ERA5 reanalysis of the evaporative fraction and temperature seasonal cycle amplitude for the period 1979–2020 (Fig. 1). We divide the Amazon basin into the four regions used by the IPCC AR6<sup>28,29</sup>, namely; North West South America (NWS), North South America (NSA), North East South America (NES), and South American Monsoon (SAM), see map. For three of the four regions the 10-year running means (solid curves) show clear decreasing trends in the evaporative fraction (blue) indicating a drying over the Amazon in recent decades. These decreasing trends in the evaporative fraction are accompanied with increasing trends in the temperature seasonal cycle amplitude (red). Individual years can also be identified (dashed timeseries), such as 2015 in the NSA region – an extreme drought event caused by a strong El Niño<sup>30</sup>. Here the anomalously high-temperature seasonal cycle amplitude coincided with an anomalously low evaporative fraction. The NWS region is the exception where there appears to be no overall trend in the temperature seasonal cycle amplitude or evaporative fraction. However, this region contains many coastal grid points and therefore evaporation is less likely to be limited by soil drying.

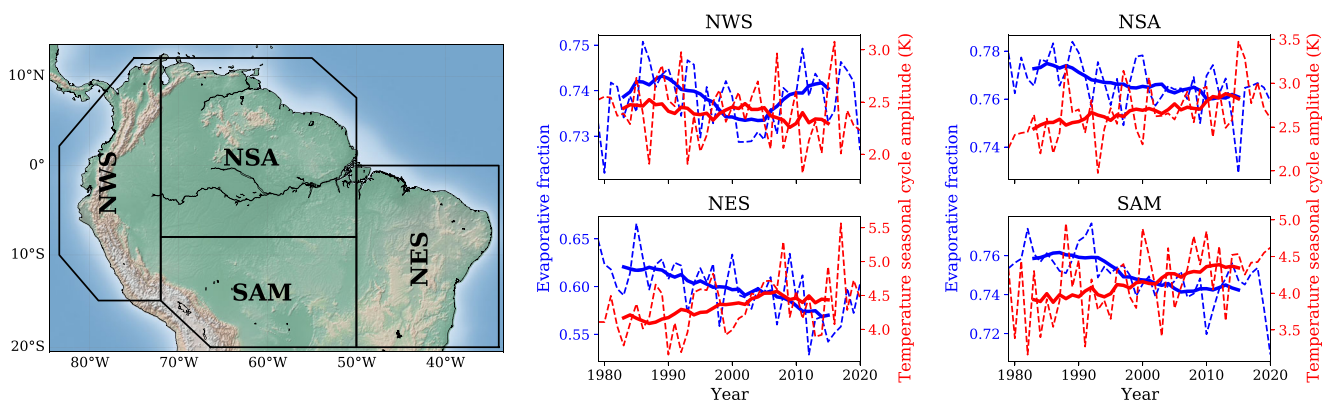


**Fig. 1 Trends in ERA5 reanalysis of evaporative fraction and temperature seasonal cycle amplitude.** Timeseries of recent annual mean values of temperature seasonal cycle amplitude and evaporative fraction for four Amazon regions (NWS–North-West South America, NSA–North South America, NES–North-East South America, SAM–South American Monsoon) depicted in the map (normalised values are also used in Fig. 3). Dashed lines are the annual values, and continuous lines are the 10-year running means.

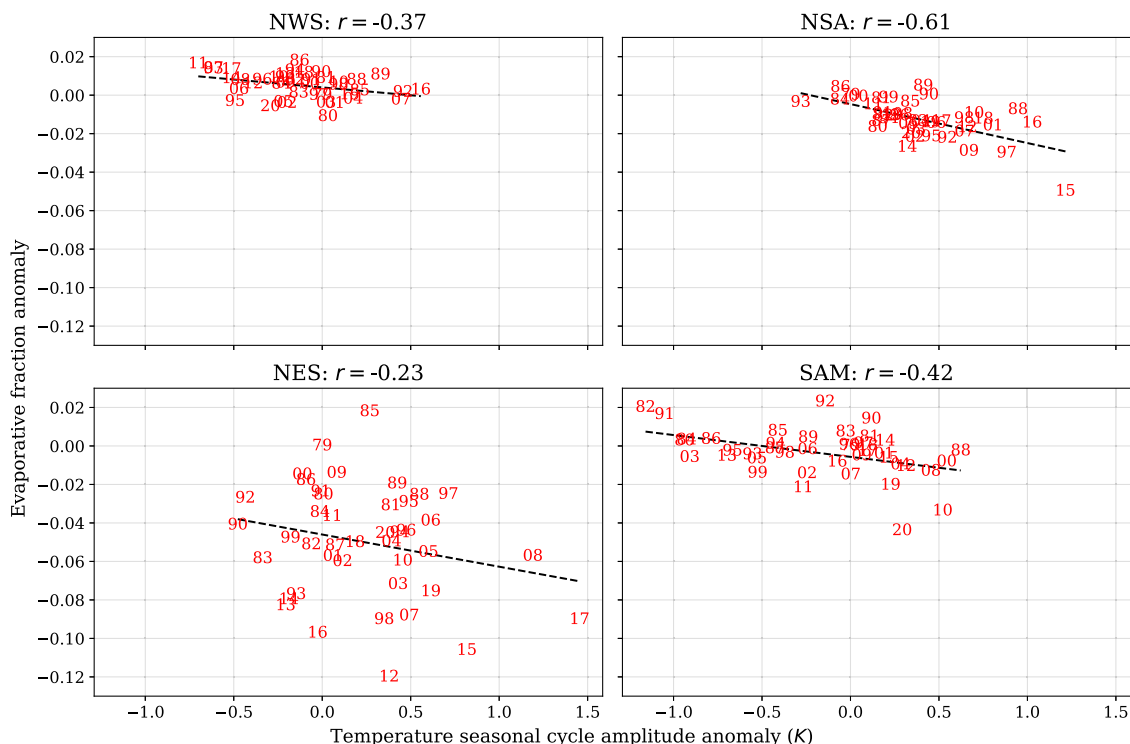


**Fig. 2 Correlations between evaporative fraction and temperature seasonal cycle amplitude in ERA5 reanalysis.** Annual mean anomalies from 1979 until 2020 in temperature seasonal cycle amplitude and evaporative fraction calculated relative to the reference year 1979. Years are marked as annotated, and for the four Amazon regions of interest (NWS, NSA, NES, and SAM). Dashed lines are the best fit regression and correlation coefficients ( $r$ ) are as annotated.

We calculate the annual anomalies in both the temperature seasonal cycle amplitude and evaporative fraction relative to the first year of the ERA5 data, 1979. These anomalies are plotted in Fig. 2, where the points are annotated by the year of the anomaly. The best fit linear regressions are given by the black dashed lines. Consistent with Fig. 1 we find a negative correlation ( $r = -0.61$ ), between temperature seasonal cycle amplitude anomalies and evaporative fraction anomalies, in the NSA region, which covers the majority of the Amazon basin. Similarly, negative correlations are also observed for the other three regions. In the NWS and NES regions, where evaporation is less limited by soil drying due to the proximity of coastal points and the Andes Mountain range, the correlations are weaker. The slope of the regression line for the NSA region implies an approximate 0.02 drop in EF for a 1 °C increase in temperature seasonal cycle amplitude. Identical analyses are performed for three alternative reanalysis products (see Figs. S1–S3 and Table S1), which also show negative correlations ( $r < -0.45$ ) for the NSA region except for JRA-55. The slopes for the NSA region range between a 0.01 to 0.07 decrease in EF for a 1 °C increase in the temperature seasonal cycle amplitude.

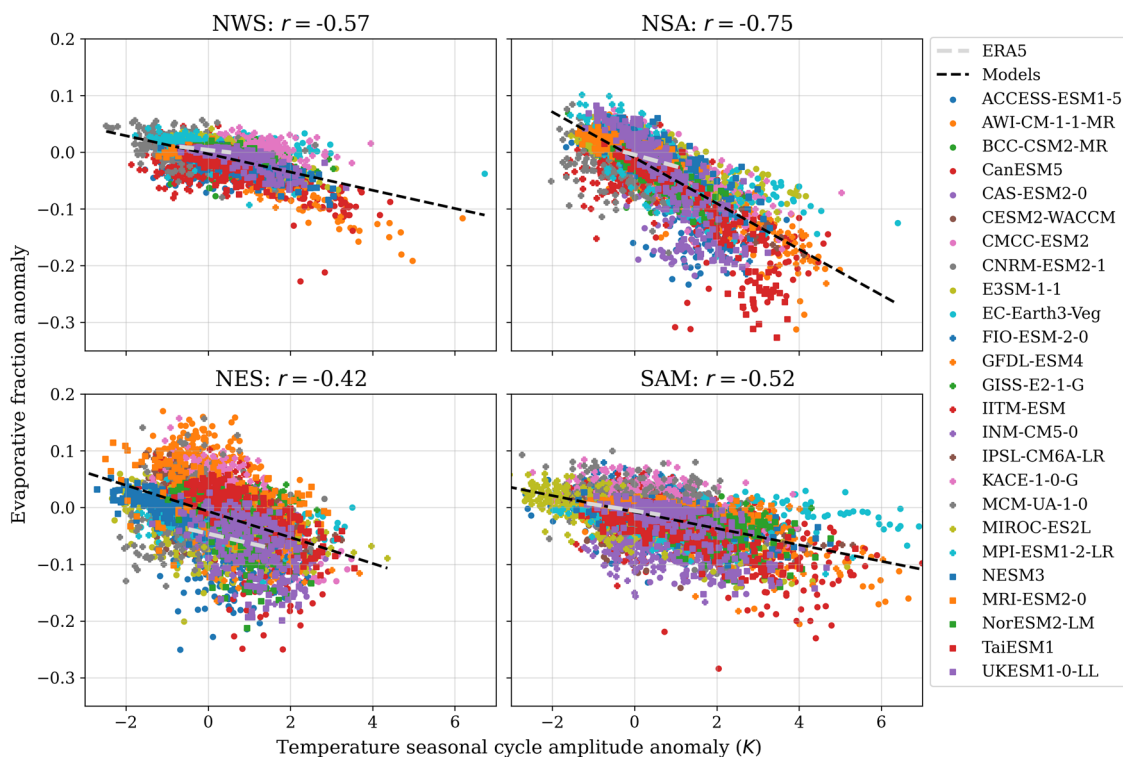
Having identified correlations between EF and the temperature seasonal cycle amplitude in the reanalysis products, we perform the same analysis for the CMIP6 dataset (Fig. 3). The added advantages of using the CMIP6 dataset is twofold. Firstly, the ability to use an ensemble of models as opposed to a single climate realisation represented by reanalysis products. Secondly, to check the EF versus temperature seasonal cycle amplitude relationship over a larger anomaly range by concatenating historical simulations with climate change projections for each model (here we use the historical and SSP5-8.5 scenarios, spanning 1900–2099, similar correlations are obtained using either the historical and SSP2-4.5 scenarios, or the idealised run of increasing CO<sub>2</sub> by 1% per year, see Figs. S4 and S5). For

comparability, the anomalies are calculated against the same reference year of 1979, as used for ERA5.

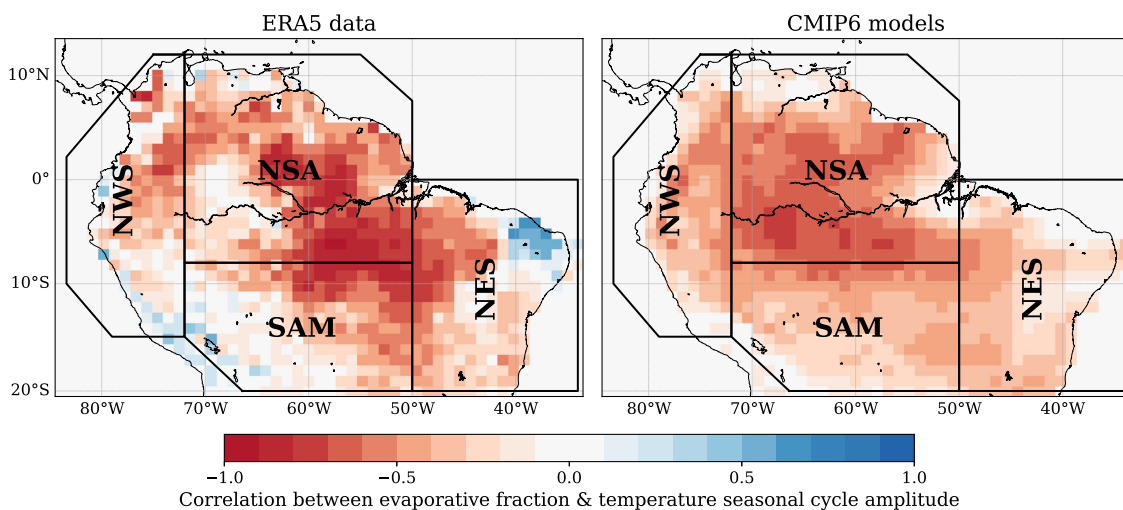
Fitting a linear regression to the CMIP6 models (black dashed lines) shows a clear negative correlation ( $r = -0.75$ ) in the NSA region. The slope of the regression for the NSA region is approximately double that derived from the ERA5 data (silver dashed line), although falls comfortably within the range of all reanalysis products. For the other three regions, stronger correlations are found in the CMIP6 dataset than for ERA5 (and generally across all reanalysis products). However, the CMIP6-derived slopes of the other three regions are notably shallower compared to the NSA region and these results are consistent irrespective of the model experiment used, as summarised by the results in Table S1. Individual CMIP6 models provide robust correlations regardless of the amount of projected drying across Amazonia. Specifically, 23 of the 25 CMIP6 models have a correlation of  $-0.5$  or stronger (and 17 of 25 have a correlation of  $-0.7$  or stronger), as shown in Table S2.

Figure 4 disaggregates this analysis onto individual grid points to investigate how the correlations vary across the regions, for both the ERA5 data and CMIP6 models. The ERA5 data shows substantial heterogeneity in the correlation between EF and temperature seasonal cycle amplitude across grid points. In central and eastern Amazonia, there is a cluster of grid points with high negative correlations. However, there are also grid points that provide positive correlations, particularly in the NWS and NES regions but also for some points in the NSA and SAM regions. Many of these positive correlations are located close to the ocean where evaporation is less likely to be limited by soil drying. The low correlations in the west of the Amazon may be indicative of the sparse distribution of observational stations in this area<sup>31</sup>.

In contrast, the correlations derived from the CMIP6 models are much more homogeneous. The vast majority of grid points display the expected negative correlation between evaporative



**Fig. 3 Modelled relation between seasonal cycle amplitude in temperature and evaporative fraction.** For the four main Amazon regions (NWS, NSA, NES, and SAM), and for ESM projections of both the historical period since 1900 and future projections under SSP5-8.5 up to 2099, we present annual anomalies (relative to the reference year 1979) in evaporative fraction as a function of near-surface temperature seasonal cycle amplitude. Each ESM uses a different combination of colour code and symbol. For each ESM, each mark is a yearly anomaly between 1900 and 2099. The black dashed line is the fitted regression across every marked point (i.e. calculated using data for each ESM and year). The overall goodness-of-fit is described by the correlation statistic,  $r$ , as annotated. The light dashed line is the regression based on ERA5 data from Fig. 2.



**Fig. 4 Regional variation in the correlation between evaporative fraction and temperature seasonal cycle amplitude.** Spatial maps of correlation coefficients for ERA5 data (left) and CMIP6 models (right). All data is based on yearly anomalies relative to the reference year 1979. ERA5 covers the period 1979–2020, and CMIP6 models 1900–2099, which is comprised of the historical period and the SSP5-8.5 scenario. The four Amazonian study regions are marked as shown.

fraction and temperature seasonal cycle amplitude. The ocean still weakens the correlation in coastal regions due to the reduced impact of soil drying on evaporative fraction, but correlations remain high ( $r < -0.5$ ) at the grid point level over the majority of the Amazon basin.

Using the relationships derived in Fig. 3 we can now reconstruct the approximate change in EF. In Fig. S6, we use the

HadCRUT5 observational temperature dataset (maroon) to reconstruct the evaporative fraction anomaly (grey) back to 1900 (before 1900 data is incomplete across the Amazon basin), relative to 1979. We compare this against the CMIP6 models EF ensemble mean given by the blue line and the shaded region indicates plus and minus one standard deviation from the mean (the same is provided in red for the CMIP6 models temperature

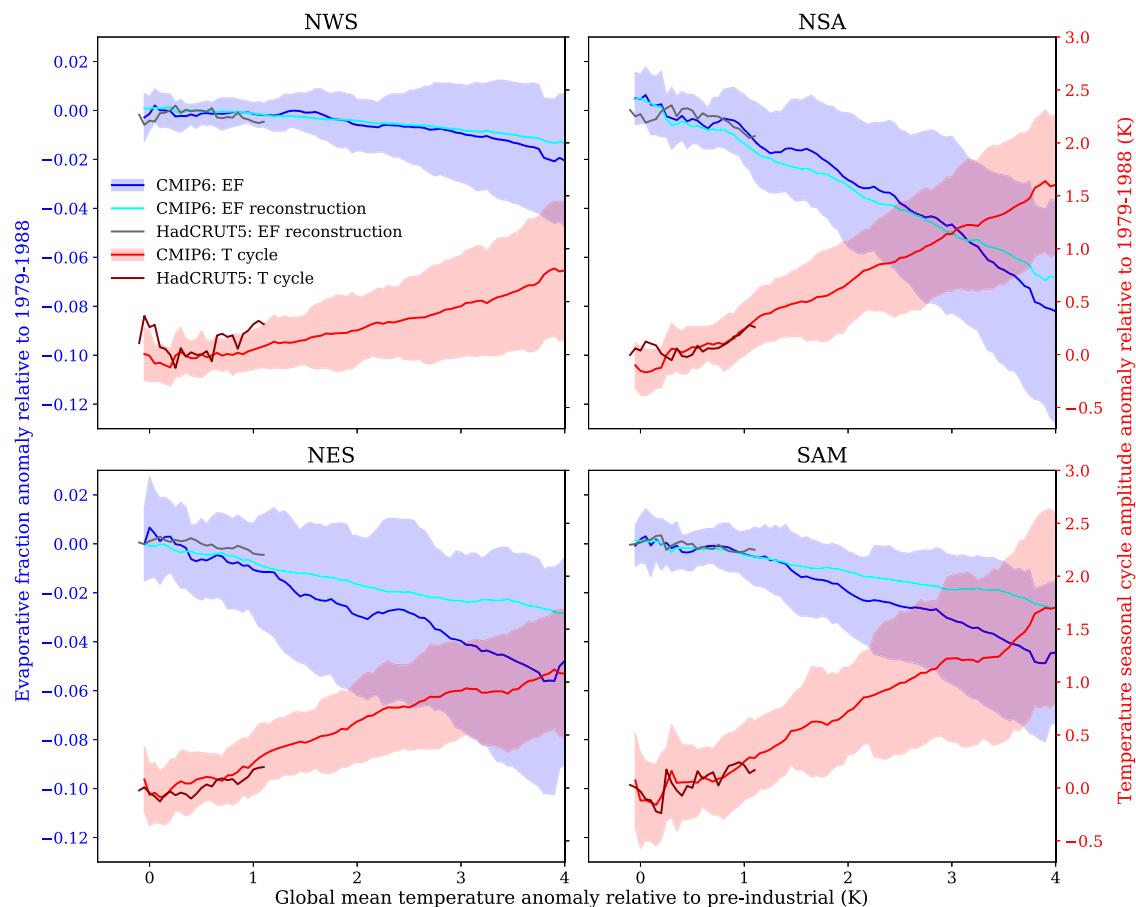


**Fig. 5 Reconstructed evaporative fraction anomaly from the temperature seasonal cycle amplitude anomaly against global warming.** Reconstruction of the evaporative fraction anomaly (calculated from the HadCRUT5 (grey) and CMIP6 model ensemble mean (light blue) temperature datasets (maroon and red respectively) using regressions calculated in Fig. 3) compared with CMIP6 model ensemble evaporative fraction mean (blue) against global warming relative to pre-industrial. Shaded regions indicate  $\pm$  one standard deviation from the CMIP6 model ensemble mean. Values are presented for the four main Amazon regions (NWS, NSA, NES, and SAM), and anomalies (relative to period 1979–88) are 10-year sliding window means plotted at the centre of the window.

seasonal cycle amplitude). However, this is dependent on the emissions scenario and gives high uncertainty partly caused by CMIP6 models having differing climate sensitivities. Therefore, in Fig. 5 we choose instead to plot against global warming over the historical period (see Methods for further details). The reconstructed evaporative fraction anomaly (smoothed over 10 years) shows a decrease under global warming in the recent past. For all four regions, the reconstructed HadCRUT5 evaporative fraction agrees well with the CMIP6 model ensemble. Furthermore, using only the temperature seasonal cycle amplitude from the CMIP6 ensemble mean, we can reconstruct the EF (light blue line) under future climate change. In all regions the CMIP6 reconstructed EF (and CMIP6 ensemble mean EF) show a clear continued drying under future global warming. For the NSA region, the reconstructed EF agrees remarkably well with the CMIP6 ensemble mean EF and indicates a substantial drying (approximate decrease in EF of 0.05) at 3 °C global warming. The EF in the NWS region is also well approximated, although for the NES and SAM regions the reconstructions slightly underestimate the drying according to the CMIP6 ensemble mean.

## Discussion

Dieback of the Amazon rainforest, as a result of regional drying and warming under anthropogenic climate change<sup>32</sup>, has long been touted as a potential tipping element in the climate

system<sup>5,6</sup>. However, previous climate model generations have failed to agree on the magnitude or even the sign of the future rainfall change in Amazonia<sup>33</sup>. Here we have presented strong evidence of a robust drying of Amazonia in the latest CMIP6 Earth System Models (ESMs), which is broadly consistent with some other recent independent assessments<sup>34–36</sup>. Consistent drying in the ERA5 climate reanalysis is also observed.

Our study has focused on the Evaporative Fraction (EF) as a dimensionless measure of surface moisture availability - reductions in EF are indicative of drying of the land surface. In the Amazon basin we find downward trends in EF in both the ERA5 climate reanalysis, and also in the historical simulations of CMIP6, for the overlapping period of 1979–2020. Furthermore, we have found a strong correlation between reductions in the annual mean EF and increases in the amplitude of the temperature seasonal cycle amplitude (mean temperature of warmest month minus mean temperature of the coolest month), which is consistent with reduced evaporative cooling in longer and more intense dry seasons in Amazonia<sup>37</sup>. Importantly, the relationship remains in both idealised runs, which do not prescribe land use changes, as well as alternative shared socioeconomic pathway scenarios, see Table S1.

Importantly, there is agreement across the CMIP6 models on correlations between the temperature seasonal cycle amplitude and EF. The vast majority of models (23 out of 25) show a correlation of  $-0.5$  or stronger in the NSA region (Table S2). The

**Table 1 List of CMIP6 models used.**

Model	Institute	Model	Institute
ACCESS-ESM1-5	Australian Community Climate and Earth System Simulator, Australia	IITM-ESM	Indian Institute of Tropical Meteorology Pune, India
AWI-CM-1-1-MR	Alfred Wegener Institute, Helmholtz Centre for Polar and Marine Research, Germany	INM-CM5-0	Institute for Numerical Mathematics, Russia
BCC-CSM2-MR	Beijing Climate Center, China	IPSL-CM6A-LR	Institut Pierre Simon Laplace, France
CanESM5	Canadian Centre for Climate Modelling and Analysis, Canada	KACE1-0-G	National Institute of Meteorological Sciences/Korea Meteorological Administration, South Korea
CAS-ESM2-0	Chinese Academy of Sciences, China	MCM-UA-1-0	University of Arizona, USA
CESM2-WACCM	National Center for Atmospheric Research, Climate and Global Dynamics Laboratory, USA	MIROC-ES2L	JAMSTEC (Japan Agency for Marine-Earth Science and Technology); AORI (Atmosphere and Ocean Research Institute); NIES (National Institute for Environmental Studies); R-CCS (RIKEN Center for Computational Science), Japan
CIesm**	Tsinghua University, Japan	MPI-ESM1-2-LR	Max Planck Institute for Meteorology, Germany
CMCC-ESM2	Fondazione Centro Euro-Mediterraneo sui Cambiamenti Climatici, Italy	NESM3	Nanjing University of Information Science and Technology, China
CNRM-ESM2-1	CNRM (Centre National de Recherches Meteorologiques); CERFACS (Centre Europeen de Recherche et de Formation Avancee en Calcul Scientifique), France	MRI-ESM2-0	Meteorological Research Institute, Japan
E3SM-1-1*	LLNL (Lawrence Livermore National Laboratory); ANL (Argonne National Laboratory); BNL (Brookhaven National Laboratory); LANL (Los Alamos National Laboratory); LBNL (Lawrence Berkeley National Laboratory); ORNL (Oak Ridge National Laboratory); PNNL (Pacific Northwest National Laboratory); SNL (Sandia National Laboratories), USA	NorESM2-LM	CICERO (Center for International Climate and Environmental Research); MET-Norway (Norwegian Meteorological Institute); NERSC (Nansen Environmental and Remote Sensing Center); NILU (Norwegian Institute for Air Research); UiB (University of Bergen); UiO (University of Oslo); UNI (Uni Research), Norway.
EC-Earth3-Veg	AEMET, BSC, University of Santiago de Compostela, Spain; CNR-ISAC, ENEA, ICTP, Italy; DMI, Denmark; FMI, University of Helsinki, Finland; Geomar, KIT, Germany; ICHEC, Met Eireann, University College Dublin, Ireland; IDL, IPMA, Portugal; IMAU, KNMI, NLeSC, surfSARA, Utrecht University, Vrije Universiteit Amsterdam, Wageningen University, The Netherlands; Lund University, SMHI, Stockholm University, Uppsala University, Sweden; NTNU, University of Bergen, Norway; Oxford University, UK; Unite ASTR, Belgium; University of Copenhagen, Denmark	SAMO-UNICON**	Seoul National University, South Korea
FIO-ESM-2-0	First Institute of Oceanography, China	TaiESM1	Research Center for Environmental Changes, Taiwan
GFDL-ESM4	NOAA Geophysical Fluid Dynamics Laboratory, USA	UKESM1-0-LL	Met Office Hadley Centre, UK
GISS-E2-1-G	Goddard Institute for Space Studies, USA		

Models are used for all three scenario runs (SSP5-8.5, SSP2-4.5, 1%CO<sub>2</sub>) unless otherwise stated. \*E3SM-1-1 used only for SSP5-8.5, alternative version E3SM-1-0 used for 1%CO<sub>2</sub>. \*\*CIesm has errors in initialisation of SSP runs; SAMO-UNICON only has data available for 1%CO<sub>2</sub> runs.

two models which display weak correlations also project the greatest wetting over the NSA region (note 22 of 25 models project drying), and under those circumstances we should indeed expect evaporation to be less limited by soil moisture, and therefore for the relationship between the temperature seasonal cycle amplitude and the EF to be much less obvious. Multiple CMIP6 models share similar components and therefore it is possible that the long-term drying trends observed could be caused by systematic bias<sup>36</sup>. However, to partly mitigate against this issue, in our analysis we select only one model per modelling centre. Additionally, the slopes of the linear regressions between the temperature seasonal cycle amplitude and EF are found to be within the range of slopes derived from the different reanalysis products.

Establishing such a strong and robust correlation has allowed us to reconstruct historical changes in EF from much longer records of near-surface temperature, indicating a continuous downward trend in EF from 1900 to the present. CMIP6 model projections suggest that this drying trend will continue with global warming, with evaporative fraction decreasing by as much

as 5% at 2 °C of global warming. Regrettably, the evidence we present gives reasons to be concerned about long-term drying in Amazonia and the potential for climate change-driven Amazon forest dieback.

## Materials and methods

**Data sources.** For this study, we utilise data from state-of-the-art climate models, reanalysis products, and observations.

We use the recently released ERA5 reanalysis data (Hersbach et al. 2020). Reanalysis datasets such as ERA5 are often considered to be the closest representation of observations, given the large number of weather station measurements that the reanalysis product entrains. However, the number of weather stations across the Amazon is relatively sparse<sup>31</sup>, and therefore their accuracy in the Amazon region is still limited. Hence, we compare the relationship between evaporative fraction and temperature seasonal cycle amplitude in the NCEP-DOE R2<sup>38</sup>, MERRA-2<sup>39</sup>, JRA-55<sup>40</sup> reanalysis products as well (see Figs. S1–S3 and Table S1).

Observational near-surface temperature from the HadCRUT5 dataset is used for reconstruction of the historical evaporative fraction anomaly<sup>41</sup>. Due to the increased number of measurements across the Amazon basin, historical temperature observational records are used from 1900 up to the end of 2020.

The climate models used are from the 6<sup>th</sup> Phase of the Coupled Model Intercomparison Project CMIP6<sup>42</sup>. See Table 1 for a full list of CMIP6 models used.

For consistency with the historical observations we use climate model output from 1900–2100, consisting of historical runs spanning 1900–2014 inclusive, which are combined with the no climate mitigation Shared Socioeconomic Pathway SSP5-8.5<sup>43</sup> to the end of the 21<sup>st</sup> century. A medium emissions scenario SSP2-4.5 and an idealised run with a prescribed 1% per year increase in atmospheric CO<sub>2</sub>, are also analysed to demonstrate the robustness of the derived relationship between evaporative fraction and temperature seasonal cycle amplitude anomalies, see Figs. S4 and S5 and Table S1.

All data is linearly interpolated onto a universal 1°x1° grid to allow direct comparison amongst CMIP6 models, reanalysis products, and observational data.

**Temperature seasonal cycle amplitude.** For the purposes of this study, the temperature seasonal cycle amplitude is defined as the difference between the minimum and maximum monthly means of each calendar year.

**Evaporative fraction.** In addition to the near-surface temperature, land-atmosphere energy flux exchanges are used to derive the evaporative fraction. Specifically, the evaporative fraction, EF, is defined as the ratio of latent heat, LE, to the available energy, which is equal to the sum of latent heat and sensible heat, H:

$$EF = \frac{LE}{LE+H}$$

**Obtaining reconstructed evaporative fraction from the temperature seasonal cycle amplitude and linking to global warming.** In this section, we provide a detailed description of the method used to generate the reconstructed evaporation fractions and subsequent links to global warming, as plotted in Fig. 5. First, we calculate annual anomalies (relative to year 1979) for the local temperature seasonal cycle amplitude, for both the HadCRUT5 data set and each CMIP6 model. We similarly calculate the local annual evaporative fraction anomalies for the individual CMIP6 models. Additionally, to assess predictive capability, we generate reconstructions of the evaporative fraction anomalies (for both HadCRUT5 and individual CMIP6 models). This reconstruction uses the relevant annual temperature seasonal cycle amplitude anomalies and linear regressions derived for each region in Fig. 3 (the black dashed lines). All anomalies, in temperature seasonal cycle amplitude and evaporative fraction are subsequently smoothed over a 10-year sliding window with a running mean and can be plotted as a time series (using the CMIP6 model mean and standard deviation for range) as shown in Fig. S6. However, presentation in this form is dependent on the selected modelled future GHG scenario and furthermore, produces a large uncertainty range partly because CMIP6 models have substantially different climate sensitivities and therefore warm at different rates. To reduce these dependencies and to make our results more relevant to the Paris global climate targets, we plot changes in South American temperature seasonal cycle amplitude and evaporative fraction against global warming (as opposed to year) in Fig. 5. Our analyses employ the measurement dataset HadCRUT5, and CMIP6 models for projections, both of which have data for both the Amazon and globally, so this is relatively straightforward to do. Specifically, we calculate global warming anomalies relative to the period 1850–1900 inclusive, for each 10-year sliding window for HadCRUT5 and the individual CMIP6 models. Applying a nearest neighbour interpolation generates local anomalies of temperature seasonal cycle amplitude and evaporative fraction on a universal array of global warming levels. This array of global warming ranges between –1 and +4 in steps of 0.05 and is used for each dataset (either HadCRUT5 or individual CMIP6 model). Importantly, no extrapolation is performed and so if a global warming level lies outside of a given dataset then no value is provided. Similarly, no values are provided for the CMIP6 ensemble mean and standard deviation banding if there are less than 10 CMIP6 model entries.

## Data availability

The datasets analysed during this study are available online: CMIP6 model output [<https://esgf-node.llnl.gov/search/cmip6/>], ERA5 reanalysis output [<https://www.ecmwf.int/en/forecasts/datasets/reanalysis-datasets/era5>], HadCRUT5 observational data [<https://www.metoffice.gov.uk/hadobs/hadcrut5/>], NCEP-DOE reanalysis output [<https://psl.noaa.gov/data/gridded/data.ncep.reanalysis2.html>], MERRA2 reanalysis output [[https://disc.gsfc.nasa.gov/datasets/M2TMNXFLX\\_5.12.4/summary?keywords=MERRA-2](https://disc.gsfc.nasa.gov/datasets/M2TMNXFLX_5.12.4/summary?keywords=MERRA-2)], JRA-55 reanalysis output [<https://rda.ucar.edu/datasets/ds628.0/>].

## Code availability

Code for reproducing the main plots of the manuscript is publicly available at [https://github.com/PaulRitchie89/CEE\\_code](https://github.com/PaulRitchie89/CEE_code).

Received: 12 May 2022; Accepted: 4 August 2022;

Published online: 01 September 2022

## References

- Brienen, R. J. W. et al. Long-term decline of the Amazon carbon sink. *Nature* **519**, 344–348 (2015).
- Pan, Y. D. et al. A large and persistent carbon sink in the world's forests. *Science* **333**, 988–993 (2011).
- Phillips, O. L. et al. Drought sensitivity of the Amazon rainforest. *Science* **323**, 1344–1347 (2009).
- Gatti, L. V. et al. Amazonia as a carbon source linked to deforestation and climate change. *Nature* **595**, 388–393 (2021).
- Lenton, T. M. et al. Tipping elements in the Earth's climate system. *Proc. Natl Acad. Sci. USA* **105**, 1786–1793 (2008).
- Cox, P. M. et al. Amazonian forest dieback under climate-carbon cycle projections for the 21st century. *Theor. Appl. Climatol.* **78**, 137–156. (2004).
- Lapola, D. M. et al. Limiting the high impacts of Amazon forest dieback with no-regrets science and policy action. *Proc. Natl Acad. Sci.* **115**, 11671–11679 (2018).
- Parry, I., Ritchie, P. & Cox, P. Evidence of Amazon rainforest dieback in CMIP6 models. EGU sphere, 2022: 1–11.
- Wainwright, C. M., Allan, R. P. & Black, E. Consistent trends in dry spell length in recent observations and future projections. *Geophys. Res. Lett.*, **49**, e2021GL097231 (2022).
- Wainwright, C. M., Black, E. & Allan, R. P. Future changes in wet and dry season characteristics in CMIP5 and CMIP6 simulations. *J. Hydrometeorol.* **22**, 2339–2357. (2021).
- Fu, R. et al. Increased dry-season length over southern Amazonia in recent decades and its implication for future climate projection. *Proc. Natl Acad. Sci.* **110**, 18110–18115 (2013).
- Espinoza, J. C. et al. Contrasting North–South changes in Amazon wet-day and dry-day frequency and related atmospheric features (1981–2017). *Clim. Dyn.* **52**, 5413–5430 (2019).
- Avila-Diaz, A. et al. Assessing current and future trends of climate extremes across Brazil based on reanalyses and earth system model projections. *Clim. Dyn.* **55**, 1403–1426 (2020).
- Barkhordarian, A. et al. Simultaneous regional detection of land-use changes and elevated GHG levels: The case of spring precipitation in tropical South America. *Geophys. Res. Lett.* **45**, 6262–6271 (2018).
- Zuidema, P. A. et al. Tropical tree growth driven by dry-season climate variability. *Nat. Geosci.* **15**, 269–276 (2022).
- Boulton, C. A., Lenton T. M. & Boers, N. Pronounced loss of Amazon rainforest resilience since the early 2000s. *Nat. Clim. Change* **12**, 271–278 (2022).
- Maes, W. H. et al. Potential evaporation at eddy-covariance sites across the globe. *Hydrol. Earth Syst. Sci.* **23**, 925–948 (2019).
- Mallick, K. et al. Canopy-scale biophysical controls of transpiration and evaporation in the Amazon Basin. *Hydrol. Earth Syst. Sci.* **20**, 4237–4264 (2016).
- Salati, E. et al. Recycling of water in the amazon basin - Isotopic study. *Water Resour. Res.* **15**, 1250–1258 (1979).
- Adams, J., *Vegetation-Climate Interaction: How Plants Make the Global Environment*. 2010, Berlin, Heidelberg: Springer. 266.
- Bathiany, S. et al. Climate models predict increasing temperature variability in poor countries. *Sci. Adv.* **4**, eaar5809 (2018).
- Good, P. et al. Nonlinear regional warming with increasing CO<sub>2</sub> concentrations. *Nat. Clim. Change* **5**, 138–142 (2015).
- Olonscheck, D. et al. Large-scale emergence of regional changes in year-to-year temperature variability by the end of the 21<sup>st</sup> century. *Nat. Commun.* **12**, 1–10 (2021).
- Donat, M. G., Pitman, A. J. & Seneviratne, S. I. Regional warming of hot extremes accelerated by surface energy fluxes. *Geophys. Res. Lett.* **44**, 7011–7019 (2017).
- Almazroui, M. et al. Assessment of CMIP6 performance and projected temperature and precipitation changes over South America. *Earth Syst. Environ.* **5**, 155–183 (2021).
- Baker, J. C. et al. Evapotranspiration in the Amazon: spatial patterns, seasonality, and recent trends in observations, reanalysis, and climate models. *Hydrol. Earth Syst. Sci.* **25**, 2279–2300 (2021).
- Hersbach, H. et al. The ERA5 global reanalysis. *Q. J. R. Meteorol. Soc.* **146**, 1999–2049 (2020).
- IPCC, *Climate Change 2021: The Physical Science Basis. Contribution of Working Group I to the Sixth Assessment Report of the Intergovernmental Panel on Climate Change*. 2021, Cambridge, United Kingdom and New York, New York, United States of America: Cambridge University Press, In Press.
- Iturbide, M. et al. An update of IPCC climate reference regions for subcontinental analysis of climate model data: definition and aggregated datasets. *Earth Syst. Sci. Data* **12**, 2959–2970 (2020).
- Jiménez-Muñoz, J. C. et al. Record-breaking warming and extreme drought in the Amazon rainforest during the course of El Niño 2015–2016. *Sci. Rep.* **6**, 1–7 (2016).

31. Condom, T. et al. Climatological and hydrological observations for the South American Andes: in situ stations, satellite, and reanalysis data sets. *Front. Earth Sci.* **8**, 92 (2020).
32. Cox, P. M. et al. Acceleration of global warming due to carbon-cycle feedbacks in a coupled climate model. *Nature* **408**, 184–187 (2000).
33. Joetzer, E. et al. Present-day and future Amazonian precipitation in global climate models: CMIP5 versus CMIP3. *Clim. Dyn.* **41**, 2921–2936 (2013).
34. Cook, B. et al. Twenty-first century drought projections in the CMIP6 forcing scenarios. *Earth's Future* **8**, e2019EF001461 (2020).
35. Ukkola, A. M. et al. Robust future changes in meteorological drought in CMIP6 projections despite uncertainty in precipitation. *Geophys. Res. Lett.* **47**, e2020GL087820 (2020).
36. Parsons, L. Implications of CMIP6 projected drying trends for 21st-century Amazonian drought risk. *Earth's Future* **8**, e2020EF001608 (2020).
37. Cintra, B. B. L. et al. Tree-ring oxygen isotopes record a decrease in Amazon dry season rainfall over the past 40 years. *Clim. Dyn.*, **59**, 1401–1414 (2021).
38. Kanamitsu, M. et al. NCEP-DOE AMIP-II reanalysis (R-2). *Bull. Am. Meteorol. Soc.* **83**, 1631–1643 (2002).
39. Rienecker, M. M. et al. MERRA: NASA's modern-era retrospective analysis for research and applications. *J. Clim.* **24**, 3624–3648 (2011).
40. Kobayashi, S. et al. The JRA-55 reanalysis: general specifications and basic characteristics. *J. Meteorol. Soc. Jpn. Ser. II* **93**, 5–48 (2015).
41. Morice, C. P. et al. An Updated Assessment of Near-Surface Temperature Change From 1850: The HadCRUT5 Data Set. *J. Geophys. Res.-Atmos.*, **126**, e2019JD032361 (2021).
42. Eyring, V. et al. Overview of the Coupled Model Intercomparison Project Phase 6 (CMIP6) experimental design and organization. *Geosci. Model Dev.* **9**, 1937–1958 (2016).
43. O'Neill, B. C. et al. The Scenario Model Intercomparison Project (ScenarioMIP) for CMIP6. *Geosci. Model Dev.* **9**, 3461–3482 (2016).

## Acknowledgements

This work was supported by the European Research Council 'Emergent Constraints on Climate-Land feedbacks in the Earth System (ECCLES)' project, grant agreement number 742472 (P.D.L.R., J.C., and P.M.C.). P.M.C. was also supported by the European Union's Framework Programme Horizon 2020 for Research and Innovation under grant agreement number 821003, Climate-Carbon Interactions in the Current Century (4C) project. C.H. acknowledges the Natural Environment Research Council National Capability Fund awarded to the UK Centre for Ecology and Hydrology. We also acknowledge the World Climate Research Programme's Working Group on Coupled Modelling, which is responsible for CMIP, and we thank the climate modelling groups

(listed in Table 1 in the Methods section) for producing and making available their model output.

## Author contributions

P.D.L.R. and P.M.C. designed and directed the research. P.D.L.R., I.P., J.J.C., C.H., and P.M.C. helped to shape the research and drafted the manuscript. P.D.L.R. performed the analysis and produced the figures.

## Competing interests

The authors declare no competing interests.

## Additional information

**Supplementary information** The online version contains supplementary material available at <https://doi.org/10.1038/s43247-022-00528-0>.

**Correspondence** and requests for materials should be addressed to Paul D. L. Ritchie.

**Peer review information** *Communications Earth & Environment* thanks the anonymous reviewers for their contribution to the peer review of this work. Primary Handling Editors: Clare Davis and Heike Langenberg. Peer reviewer reports are available.

**Reprints and permission information** is available at <http://www.nature.com/reprints>

**Publisher's note** Springer Nature remains neutral with regard to jurisdictional claims in published maps and institutional affiliations.



**Open Access** This article is licensed under a Creative Commons Attribution 4.0 International License, which permits use, sharing, adaptation, distribution and reproduction in any medium or format, as long as you give appropriate credit to the original author(s) and the source, provide a link to the Creative Commons license, and indicate if changes were made. The images or other third party material in this article are included in the article's Creative Commons license, unless indicated otherwise in a credit line to the material. If material is not included in the article's Creative Commons license and your intended use is not permitted by statutory regulation or exceeds the permitted use, you will need to obtain permission directly from the copyright holder. To view a copy of this license, visit <http://creativecommons.org/licenses/by/4.0/>.

© The Author(s) 2022